

**GROWTH AND CHARACTERIZATION OF VERTICALLY
ALIGNED ZnO NANORODS SYNTHESIZED BY CHEMICAL
BATH DEPOSITION FOR UV PHOTODETECTOR
APPLICATIONS**

By

REZA SHABANNIARAMI

**Thesis submitted in fulfillment of the
requirements for the degree of
Doctor of Philosophy**

UNIVERSITI SAINS MALAYSIA

December 2013

DEDICATION

TO

MY PARENTS, MY BROTHERS, MY SISTERS,

MY SON AND MY WIFE

ACKNOWLEDGEMENTS

First and foremost, I would like to thank Allah for granting me good health and patience to complete this research. I would also like to express sincere gratitude to my main supervisor, Prof. Dr. Haslan Abu Hassan for his intellectual guidance; devoted time and support in completing this study. I also express my gratitude to my friends Dr. N. Naderi, M. Alimanesh, H. Mahmodi, Dr. J. Rohi, Dr. G. Alahyarizadeh, A. Farhadi, A. Soltani, A. Shirinzadeh, E. Yosefi, M. Ghasemtabar, and all my other friends especially in School of Physics, USM who help and guided me at all time during my study. I also express appreciation to the staff of the Nano-Optoelectronics Research and Technology Laboratory (NOR Lab) and of the Solid-state Laboratory for their technical assistance during my laboratory work, particularly in the sample characterizations. I would like to express my gratitude to my dear parents, my brothers, and my sisters for their unconditional love and support. I would like to thank my wife for giving me their great love, endless support, sympathy and encouragement when I needed it, and especially for taking care of my lovely son Mahdiar during my pursuit of my doctoral study. Finally, my deepest and heartfelt gratitude goes to my son for his patience while I took time away from him for my studies and writing this thesis.

TABLE OF CONTENTS

	Pages
DEDICATION	ii
ACKNOWLEDGEMENTS	iii
TABLE OF CONTENTS	iv
LIST OF TABLES	x
LIST OF FIGURES	xi
LIST OF ABBREVIATIONS	xv
LIST OF SYMBOLS	xvii
ABSTRAK	xix
ABSTRACT	xxi
CHAPTER 1: INTRODUCTION	
1.1 Introduction	1
1.2 Motivation and problem statement	2
1.3 Scope of study	3
1.4 Objectives of thesis	3
1.5 Originality of thesis	4
1.6 Outline of thesis	4
CHAPTER 2: LITERATURE REVIEW AND BACKGROUND	
2.1 Introduction	6
2.2 Nanomaterials	6

2.3	Overview of ZnO and ZnO nanostructures	7
	2.3.1 Crystal structures and lattice parameters of ZnO	8
	2.3.2 Optical properties of ZnO	11
2.4	Overview of substrates	12
	2.4.1 Flexible polyethylene naphthalate (PEN) substrate	13
	2.4.2 Porous silicon (PS) substrate	14
2.5	Overview of chemical bath deposition technique	15
	2.5.1 The chemical bath deposition technique	15
	2.5.2 Mechanism of chemical bath deposition technique	18
2.6	Overview of ZnO nanorods growth conditions	19
	2.6.1 Mechanism of ZnO nanorods growth conditions	19
	2.6.2 Literature review	20
2.7	Overview of ultraviolet (UV) photodetection based on ZnO nanorods	22
	2.7.1 Literature review	23
	2.7.2 Theoretical concepts of ultraviolet detection	24
	2.7.2.1 Photoconductivity	26
	2.7.2.2 Typical mechanism of photoconduction in ZnO nanorods	30

CHAPTER 3: EXPERIMENTAL AND CHARACTERIZATION TOOLS

3.1	Photo electrochemical etching (PECE) cell	32
3.2	Radio frequency (RF)/direct current (DC) sputtering system	32
3.3	Thermal annealing processes	33
3.4	Principles of the characterization tools	34
	3.4.1 Structural tools	35

3.4.1.1 X -ray diffraction (XRD)	35
3.4.1.2 Field emission scanning electron microscopy (FESEM)	37
3.4.1.3 Energy dispersive X-ray analysis (EDX)	39
3.4.1.4 Transmission electron microscopy (TEM)	39
3.4.1.5 Atomic force microscopy (AFM)	41
3.4.2 Tools used for the optical characterization of ZnO nanorods	42
3.4.2.1 Photoluminescence (PL) spectroscopy	42
3.4.2.2 Raman spectroscopy	44
3.4.2.3 Optical reflectometer	46
3.4.3 Current-voltage and current-time measurements system	47

CHAPTER 4: METHODOLOGY

4.1	Introduction	48
4.2	Preparation of substrates	48
	4.2.1 Preparation and cleaning of polyethylene naphthalate substrate	48
	4.2.2 Preparation and cleaning of porous silicon substrate	48
4.3	Deposition of ZnO seed layer on prepared substrates	50
4.4	Annealing process of ZnO seed layer	51
4.5	Synthesis of ZnO nanorods using chemical bath deposition technique	51
4.6	Structural and optical characterizations	53
4.7	Fabrication of ultraviolet photodetector	53
4.8	Measurements of ultraviolet photodetector	53

CHAPTER 5: ZnO NANORODS ON POLYETHYLENE NAPHTHALATE SUBSTRATE

5.1	Growth and characterization of ZnO nanorods with different precursor concentrations	55
5.1.1	Introduction	55
5.1.2	Atomic force microscopy observation	56
5.1.3	X-ray diffraction analysis	56
5.1.4	Surface morphology	59
5.1.5	Transmission electron microscopy image of ZnO nanorods	62
5.1.6	Photoluminescence spectra	63
5.2	Growth and characterization of ZnO nanorods with different growth durations	66
5.2.1	Introduction	66
5.2.2	Atomic force microscopy observation	66
5.2.3	X-ray diffraction analysis	67
5.2.4	Surface morphology	69
5.2.5	Transmission electron microscopy image of ZnO nanorods	71
5.2.6	Photoluminescence measurements	72
5.3	Summary	74
CHAPTER 6: ZnO NANORODS ON POROUS SILICON SUBSTRATE		
6.1	Growth and characterization of ZnO nanorods with different precursor concentrations	76
6.1.1	Introduction	76
6.1.2	Atomic force microscopy observation	77
6.1.3	X-ray diffraction analysis	78
6.1.4	Field emission scanning electron microscopy observation	80
6.1.5	Transmission electron microscopy image of ZnO nanorods	83
6.1.6	Photoluminescence measurements	84

6.1.7	Raman spectra	87
6.2	Growth and characterization of ZnO nanorods with different growth durations	88
6.2.1	Introduction	88
6.2.2	Atomic force microscopy observation	89
6.2.3	X-ray diffraction analysis	90
6.2.4	Field emission scanning electron microscopy observation	92
6.2.5	Transmission electron microscopy image of ZnO nanorods	93
6.2.6	Photoluminescence measurements	94
6.2.7	Raman spectra	96
6.3	Summary	98

CHAPTER 7: ULTRAVIOLET PHOTODETECTOR

7.1	Ultraviolet photodetector based on ZnO nanorods grown on flexible polyethylene naphthalate substrate	100
7.1.1	Introduction	100
7.1.2	Characterization of ZnO nanorods grown on polyethylene naphthalate substrate	101
7.1.3	Ultraviolet photodetection by ZnO nanorods on polyethylene naphthalate substrate	101
7.2	Ultraviolet photodetector based on ZnO nanorods grown on porous silicon substrate	105
7.2.1	Introduction	105
7.2.2	Characterization of ZnO nanorods grown on porous silicon substrate	105
7.2.3	Ultraviolet photodetection by ZnO nanorods on porous silicon substrate	106
7.3	Summary	109

CHAPTER 8: CONCLUSIONS AND FUTURE WORKS

8.1	Conclusions	111
8.2	Future work	113
REFERENCES		114
PUBLICATIONS		
	International Journals	128
	International Conferences	128

LIST OF TABLES

	Page
Table 2.1: Summary of the ZnO nanostructures synthesized using CBD method.	18
Table 2.2: Summary of photoelectrical parameters of 1D UV photodetector devices as reported in the literature.	25
Table 4.1: RF sputtering conditions for ZnO seed layer on PEN and PS substrates.	51
Table 5.1: A detail of XRD patterns of ZnO nanorods with different precursor concentrations.	58
Table 5.2: Summarized data from PL spectra of ZnO nanorods.	65
Table 5.3: A detail of XRD results of ZnO nanorods under various growth times.	69
Table 6.1: Summarized data from XRD peaks of ZnO nanorods under various precursor concentrations.	80
Table 6.2: Summarized data from PL spectra of aligned ZnO nanorods.	87
Table 6.3: Summarized data from XRD patterns of aligned ZnO nanorods.	91
Table 6.4: Summarized data from FESEM images of aligned ZnO nanorods.	93
Table 6.5: Summarized data from PL spectra of aligned ZnO nanorods.	96
Table 7.1: Photoelectrical parameters of UV photodetector in the current study and the values obtained from reported UV photodetectors in the literature.	104
Table 7.2: Photoelectrical parameters of ZnO nanorods photodetector device in the current study and the values obtained from reported ZnO nanorod photodetectors in the literature.	108

LIST OF FIGURES

	Page
Figure 2.1:	(a) The hexagonal wurtzite structure and (b) hexagonal unit cell of ZnO. 9
Figure 2.2:	(a) Miller indices of several lattice planes in a hexagonal lattice and (b) hexagonal unit cell and indices of several lattice directions. 10
Figure 2.3:	(a) The rock salt and (b) zincblende structures of ZnO. 10
Figure 2.4:	Schematic illustration of the simple photoconductor with an applied external bias voltage V . 26
Figure 2.5:	Schematic of the photoconduction in a ZnO nanowire photodetector: (a) schematic of a ZnO nanowire photodetector, (b) schematic of oxygen-trapping mechanism in ZnO nanowire in dark, and (c) schematic of hole-trapping and photoconduction mechanism in ZnO nanowire under UV illumination. 31
Figure 3.1:	Schematic of the electrochemical etching cell used to generate porous silicon. 32
Figure 3.2:	Schematic of the RF/DC sputtering system. 33
Figure 3.3:	Schematic of a thermal annealing tube furnace. 34
Figure 3.4:	Experimental setup of the HR-XRD system. 35
Figure 3.5:	A schematic of FESEM configuration. 37
Figure 3.6:	Image of the FESEM system. 38
Figure 3.7:	Schematic diagram of a typical TEM system. 40
Figure 3.8:	Schematic of electron optics diagram of TEM system in (a) imaging and (b) diffraction modes. 40
Figure 3.9:	A schematic of atomic force microscopy (AFM) configuration. 41
Figure 3.10:	PL instrument setup configuration. 42
Figure 3.11:	The E_a , E_d and E_i reveal the energy level of acceptor, donor and intermediate, respectively. (a-d) show the radiative recombination processes and (e) shows the non-radiative recombination, respectively. 43

Figure 3.12:	Schematic diagrams of the two types of scattering processes. The v_f and v_i are final and initial states, respectively.	45
Figure 3.13:	A schematic of Raman spectroscopy system.	46
Figure 3.14:	Photograph of Optical reflectometry system (Filmetrics F20).	47
Figure 4.1:	Flow chart of the fabrication processes for ZnO nanorods grown on seed layers ZnO/PEN and ZnO/PS, and UV photodetector devices.	49
Figure 4.2:	Schematic illustration of the ZnO nanorods in an oven.	52
Figure 4.3:	Top view SEM image of the ZnO nanorods MSM photodetector.	54
Figure 4.4:	Schematic diagram of the experimental set-up for UV photoresponse measurement.	54
Figure 5.1:	Three-dimensional view of AFM image of ZnO seed layer on the PEN substrate.	56
Figure 5.2:	XRD patterns of the ZnO nanorods grown on seed layer ZnO/PEN under different precursor concentrations: (a) 0.025 M, (b) 0.050 M, (c) 0.075 M, and (d) 0.100 M.	58
Figure 5.3:	FESEM images and diameter distributions of the ZnO nanorods grown on seed layer ZnO/PEN under different precursor concentrations: (a) and (b) 0.025 M, (c) and (d) 0.050 M.	59
Figure 5.4:	FESEM images and diameter distributions of the ZnO nanorods grown on seed layer ZnO/PEN under different precursor concentrations: (a) and (b) 0.075 M, (c) and (d) 0.100 M.	60
Figure 5.5 :	EDX spectrum of aligned ZnO nanorods grown on ZnO/PEN substrate.	62
Figure 5.6:	(a) Low resolution TEM image and (b) high resolution TEM image of the ZnO nanorods. The inset is the SAED pattern from an individual ZnO nanorod.	63
Figure 5.7:	Room temperature PL spectra of the ZnO nanorods grown on seed layer ZnO/PEN under different precursor concentrations: (a) 0.025 M, (b) 0.050 M, (c) 0.075 M, and (d) 0.100 M, (e) room temperature PL spectrum of bare PEN substrate, and (f) UV peak FWHM and NBE/DLE peak ratio.	64
Figure 5.8:	Three-dimensional view of AFM image of ZnO seed layer on the PEN substrate.	67

Figure 5.9:	XRD patterns of the ZnO nanorods with various growth durations: (a) 2 h, (b) 3.5 h, (c) 5 h, (d) 6.5 h and (e) 8 h.	68
Figure 5.10:	Surface FESEM images of the ZnO nanorod arrays with different growth durations: (a) 2 h, (b) 3.5 h, (c) 5 h, (d) 6.5 h and (e) 8 h.	70
Figure 5.11:	Low magnification TEM image of the ZnO nanorods grown for 8 h.	71
Figure 5.12:	PL spectra of ZnO nanorod arrays with various growth times: (a) 2 h, (b) 3.5 h, (c) 5 h, (d) 6.5 h and (e) 8 h.	73
Figure 6.1:	Three-dimensional view of AFM image of ZnO seed layer on the PS substrate.	77
Figure 6.2:	XRD patterns of the ZnO nanorods with various precursor concentrations: (a) 0.025, (b) 0.050, (c) 0.075 M, and 0.100 M.	79
Figure 6.3:	Cross section and surface FESEM images of the ZnO nanorod arrays with different precursor concentrations: (a) 0.025 M, (b) 0.050 M, (c) 0.075 M, and (d) 0.100 M.	81
Figure 6.4:	EDX spectrum of aligned ZnO nanorods grown on ZnO/PS substrate.	83
Figure 6.5:	(a) Low resolution TEM image of the ZnO nanorods and (b) high resolution TEM image showing the high crystallinity of a ZnO nanorod. The inset is the SAED pattern from an individual ZnO nanorod.	84
Figure 6.6:	PL spectra of aligned ZnO nanorods with various precursor concentrations: (a) bare PS substrate, (b) 0.025 M, (c) 0.050 M, (d) 0.075 M, (e) 0.100 M, and (f) the intensity ratio of UV light emission to visible light emission ($I_{UV}/I_{Visible}$).	85
Figure 6.7:	Raman spectra of the ZnO nanorods with various precursor concentrations: (a) 0.025 M, (b) 0.050 M, (c) 0.075 M, and 0.100 M.	88
Figure 6.8:	Three-dimensional view of AFM image of ZnO seed layer on the PS substrate.	89
Figure 6.9:	XRD patterns of the aligned ZnO nanorods with various growth durations: (a) 2, (b) 3.5, (c) 5, (d) 6.5 and (e) 8 h.	90
Figure 6.10:	Cross section and surface FESEM images of the aligned ZnO nanorods with different growth durations: (a) 2 h, (b) 3.5 h, (c) 5 h, (d) 6.5 h, and (e) 8 h.	92

Figure 6.11:	Low magnification TEM image of the ZnO nanorods grown for 5 h.	94
Figure 6.12:	PL spectra of aligned ZnO nanorods with various growth durations: (a) 2 h, (b) 3.5 h, (c) 5 h, (d) 6.5 h, (e) 8 h, and (f) the intensity ratio of UV light emission to visible light emission ($I_{UV}/I_{Visible}$).	95
Figure 6.13:	Raman spectra of aligned ZnO nanorods with various growth duration: (a) 2 h, (b) 3.5 h, (c) 5 h, (d) 6.5 h, and (e) 8 h.	97
Figure 7.1:	Current-voltage characteristics of the ZnO nanorods photodetector measured in dark and under UV illumination. The inset shows the Pt finger contacts on top of the ZnO nanorods.	102
Figure 7.2:	Photoresponse time of the fabricated UV photodetector at 3 V bias voltage.	104
Figure 7.3:	Three-dimensional view FESEM images of the ZnO nanorods on PS substrate.	106
Figure 7.14:	Current-voltage characteristics of the ZnO nanorods photodetector measured in dark and under UV (325 nm) illumination.	107
Figure 7.5:	Photoresponse time of the fabricated ZnO UV photodetector at 1 V bias voltage.	109

LIST OF ABBREVIATIONS

a.u.	Arbitrary unit
AFM	Atomic force microscopy
CCD	Charge coupled device
CBD	Chemical bath deposition
CVD	Chemical vapor deposition
CB	Conduction band
I-T	Current-Time
I-V	Current-Voltage
DLE	Deep-level emission
DI	Deionized
DC	Direct current
EDX	Energy dispersive X-ray
eV	Electron volt
FESEM	Field emission scanning electron microscopy
FTO	Fluorine doped tin oxide
FWHM	Full width at half maximum
HMT	Hexamethylenetetramine
HR-XRD	High resolution-X ray diffraction
HR-TEM	High resolution-transmission electron microscopy
ITO	Indium tin oxide
LED	Light emitting diode
LO	Longitudinal optic
MOCVD	Metal organic chemical vapor deposition

MSM	Metal-semiconductor-metal
MBE	Molecular beam epitaxy
NBE	Near band emission
PECE	Photo electrochemical etching
PL	Photoluminescence
PVD	Physical vapor deposition
PC	Polycarbonate
PEN	Polyethylene naphthalate
PES	Polyethersulfone
PET	Polyethylene terephthalate
PI	Polyimide
PS	Porous silicon
RCA	Radio corporation of America (cleaning procedure)
RF	Radio frequency
RT	Room temperature
C_{6v}^4	Schoenflies notation of space group of hexagonal ZnO
TEM	Transmission electron microscopy
TO	Transverse optic
UV	Ultraviolet
Vis	Visible
XRD	X-ray diffraction

LIST OF SYMBOLS

A	Area
D	Average crystal size
q	Charge of electron
σ_0	Conductivity in dark
σ	Conductivity in the presence of light
I_0	Current in dark
I	Current in the presence of light
J	Current density
J_n	Current density of electron
J_p	Current density of hole
E_C	Conduction band
I_{dark}	Dark current
E	Electric field
n_0	Electron concentration at equilibrium
μ_n	Electron mobility
E_g	Energy gap
E_a	Energy level of acceptor
E_d	Energy level of donor
E_i	Energy level of intermediate
ν	Frequency of light
E_F	Fermi level of semiconductor
ν_f	Final state

p_0	Hole concentration at equilibrium
μ_p	Hole mobility
θ	Incident / Diffraction angle
v_i	Initial state
d	Interplanar spacing of the crystal planes
a	Lattice constant
c	Lattice constant
τ_n	Lifetime of carriers
(hkl)	Miller indices
G_0	Net optical generation rate
P_{opt}	Optical power of the incident light
I_{ph}	Photocurrent
S	Photosensitivity
η	Quantum efficiency
R_λ	Responsivity of photodetector
ε_{zz}	Strain along c-axis
t	Time
τ_t	Transit time of carriers
Δ	Thermal energy
V	Voltage
λ	Wavelength
w	Width

**PENUMBUHAN DAN PENCIRIAN RODNANO ZnO TERJAJAR
MENEGAK YANG DISINTESIS OLEH PEMENDAPAN MANDIAN KIMIA
BAGI PENGGUNAAN SEBAGAI PENGESANFOTO UV**

ABSTRAK

Objektif-objektif dalam kajian ini adalah menumbuh dan mencirikan sifat struktur, optik dan elektrik rod nano ZnO terjajar, dan membangun pengesanfoto ultraungu (UV) menggunakan susunatur rod nano ZnO ini yang ditumbuh menggunakan parameter-parameter penumbuhan yang dioptimumkan. Kajian ini menggunakan dua substrat berbeza bagi penumbuhan susunatur rod nano ZnO, pertama, polietilena naphthalate (PEN) fleksibel dan kedua, silikon berliang (PS). Dalam kajian pertama, susunatur rod nano ZnO terjajar baik ditumbuhkan di atas substrat fleksibel PEN pada suhu rendah menggunakan pemendapan mandian kimia (CBD). Kawalan bagi diameter, panjang, ketumpatan, dan sifat optik dan struktur susunatur rod nano ZnO telah dikaji secara sistematik dengan mengubahsuai parameter penumbuhan, merangkumi kepekatan prekursor dan tempoh penumbuhan. Susunatur rod nano ZnO terjajar menegak yang ditumbuh menggunakan kepekatan prekursor 0.050 M dan tempoh penumbuhan 5 jam mempunyai diameter dalam julat 10 nm ke 40 nm dan mempamerkan puncak UV paling tajam dan berkeamatan tinggi bagi keputusan fotoluminesens (PL) pada suhu bilik dibandingkan dengan sampel yang lain. Seterusnya, susunatur rod nano ZnO berkualiti tinggi disintesis menerusi pengoptimuman kepekatan prekursor dan tempoh penumbuhan menggunakan kaedah CBD di atas substrat PS yang telah disediakan menerusi kaedah punaran foto elektrokimia (PECE). Rod nano ZnO terjajar tumbuh seranjang dengan substrat PS dan mempunyai diameter dan panjang masing-masing dalam julat 13 nm ke 69 nm

dan 85 nm ke 208 nm. Analisis PL dan Raman bagi sampel yang telah dioptimumkan (dengan 0.050 M dan 5 jam) masing-masing mempamerkan nisbah tertinggi keamatan pancaran berhampiran pinggir jalur dengan pancaran jalur hijau dan keamatan paling tinggi mod fonon E2 (tinggi) dibandingkan dengan sampel yang lain. Akhir sekali, pengesanfoto UV logam-semikonduktor-logam berasaskan susunatur rod nano ZnO yang telah dioptimumkan telah difabrikasikan di atas substrat PEN dan PS. Ciri-ciri optoelektronik pengesanfoto yang telah difabrikasi dikaji dalam keadaan gelap dan di bawah pencahayaan cahaya UV 325 nm. Pengesanfoto UV fleksibel yang terdiri daripada rod nano ZnO di atas substrat PEN menunjukkan kesambutan tinggi bernilai 2.856 A/W dan kepekaanfoto 11.75, sementara fotopengesan UV yang difabrikasi dengan rod nano ZnO terjajar menegak di atas substrat PS mempamerkan sambutan pantas dan masa pemulihan masing-masing bernilai 58 ms dan 72 ms.

**GROWTH AND CHARACTERIZATION OF VERTICALLY ALIGNED ZnO
NANORODS SYNTHESIZED BY CHEMICAL BATH DEPOSITION FOR
UV PHOTODETECTOR APPLICATIONS**

ABSTRACT

The objectives of this study are to grow and characterize the structural, optical, and electrical properties of aligned ZnO nanorods, and to develop ultraviolet (UV) photodetectors using these ZnO nanorod arrays grown with optimized growth parameters. The study employed two different substrates for growing ZnO nanorod arrays; first, flexible polyethylene naphthalate (PEN) seeded ZnO and second, porous silicon (PS) seeded ZnO. Well-aligned ZnO nanorod arrays were grown on flexible PEN substrates at a low temperature by using the chemical bath deposition (CBD). The control of the diameter, length, density, and optical and structural properties of the ZnO nanorod arrays were systematically investigated by modifying the growth parameters, including the precursor concentration and growth duration. Vertically aligned ZnO nanorod arrays grown using a 0.050 M precursor concentration and 5 h growth duration had diameters ranging from 10 nm to 40 nm and exhibited the sharpest and most intense UV peak in the room temperature photoluminescence (PL) results compared with other samples. Next, high quality ZnO nanorod arrays were synthesized through the optimization of precursor concentration and growth duration by using CBD method on PS substrates, which were prepared via the photo electrochemical etching (PECE) method. The aligned ZnO nanorods grew perpendicular to the PS substrates and had average diameters and lengths ranging from 13 nm to 69 nm and from 85 nm to 208 nm, respectively. The PL and Raman analyses of optimized sample (with 0.050 M and 5 h) exhibited highest near band

edge emission to green band emission intensity ratio and most intense E_2 (high) phonon mode compared with other samples, respectively. Finally, metal–semiconductor-metal UV photodetectors based on optimized ZnO nanorod arrays were fabricated on the PEN and PS substrates. The optoelectronic characteristics of the fabricated UV photodetectors were studied in the dark and under 325 nm UV light illumination. The flexible UV photodetector of ZnO nanorods on PEN substrate showed a high responsivity of 2.856 A/W and photosensitivity of 11.75 , while, UV photodetector fabricated with vertically aligned ZnO nanorods grown on PS substrate exhibited fast response and recovery times of 58 ms and 72 ms, respectively.

CHAPTER 1

INTRODUCTION

1.1 Introduction

Zinc oxide (ZnO) nanostructures are intrinsically n-type semiconductors with a wide direct band gap of 3.37 eV and a large exciton binding energy of 60 meV; thus, they have interesting properties such as high thermal and mechanical stabilities, unique optical and electronic properties [1]. ZnO nanostructure is a versatile functional material that exists in various growth morphologies such as nanorings, nanobelts, nanotubes, nanospheres, nanowires, nanorods, and flowers-like structures. One-dimensional ZnO nanostructures have drawn much attention in last decade because of their slow electron/hole recombination rate, faster response, high surface-to-volume ratio, specific crystalline orientation, and higher optical gain. Therefore, production of ZnO nanorods characterized by diverse morphologies and diameter size is of major significance for the fundamental research and development of novel electronic and optoelectronic devices such as photodetectors [2], field-effect transistors [3], chemical sensors [4], next-generation UV sources, solar cells [5], light-emitting diodes [6], and nanogenerators [7]. A number of techniques such as hydrothermal [8], electrochemical deposition [9], pulsed laser deposition [10], and chemical bath deposition [11], metal organic chemical vapor deposition [12], have been utilized to produce ZnO nanorods on various types of substrates.

1.2 Motivation and problem statement

To date, many studies have been conducted to fabricate ZnO nanostructures on different substrates such as silicon, glass, sapphire and many others. Fabrication of ZnO nanostructures on silicon substrate has attracted huge interest because of their lower cost and larger area size compared with sapphire substrate, which is quite expensive with smaller area size. A large stress exists between the ZnO nanostructures and Si substrates due to the large mismatches in their respective lattice constants and thermal expansion coefficients.

Recently, flexible polymer substrates because of their interesting properties such as transparency, low weight, thinness, transportability, and high resistance to impact damage have been used for production of portable devices. With the increasing demand for convenient and portable applications, flexible polymer substrates are more useful compared with conventional rigid substrates such as silicon, glass and sapphire.

Most synthesis methods for nanostructured ZnO require high temperatures. High temperature synthesis methods consume more energy and require expensive, complex instruments, which raise the production cost of ZnO-based devices. The central problem in low-temperature growth methods for ZnO nanorods/nanowires is the high concentration of defects states that lead to the low structural and optical quality of the prepared ZnO nanorods/nanowires.

The chemical bath deposition was used for mass production of ZnO nanostructures with good controls of morphology and composition because of its low

temperature process, more environmentally friendly chemicals used, lower cost, and capability for large-scale production.

1.3 Scope of study

This study optimized the growth parameters such as precursor concentration and growth duration to produce vertically aligned ZnO nanorods on polyethylene naphthalate (PEN) and porous silicon (PS) substrates using low temperature chemical bath deposition (CBD) method. The structural and optical optimizations were done by AFM, XRD, FESEM, TEM, PL and Raman spectroscopy at room temperature. The optimized ZnO nanorods on PEN and PS substrates were used to fabricate photodetectors with enhanced UV light illumination performance.

1.4 Objectives of thesis

The main objectives of this thesis can be summarized in the following points:

1. Produce and characterization of vertically aligned ZnO nanorods synthesized on PEN and PS substrates using low temperature CBD technique.
2. To evaluate the effect of changing the precursor concentration and growth time on the structural and optical properties of the aligned ZnO nanorod arrays synthesized on PEN and PS substrates.
3. To determine optimal growth parameters that control the morphology and size of the aligned ZnO nanorod arrays using modifying precursor concentration and growth duration for enhancing the device performance.
4. To produce and verify two performance of metal-semiconductor-metal (MSM) UV photodetectors based on the aligned ZnO nanorods on PEN and PS substrates.

1.5 Originality of thesis

The originality of this research work involves the following aspects:

1. The growth of vertically aligned ZnO nanorods with very small diameter and high structural and optical qualities on flexible PEN substrate.
2. The synthesis of vertical and high-density ZnO nanorod arrays on PS substrate by low temperature CBD technique for the first time, to the best of our knowledge.
3. The study of precursor concentration effect on the structural and optical properties of aligned ZnO nanorod arrays synthesized on PEN and PS substrates.
4. The investigation of growth time effect on the structural and optical properties of aligned ZnO nanorod arrays synthesized on PEN and PS substrates.
5. Fabrication of high responsivity UV photodetector based on ZnO nanorods grown on PEN substrate.
6. Fabrication of high sensitivity and very fast photoresponse of a UV photodetector based on ZnO nanorods grown on PS substrate.

1.6 Outline of thesis

Chapter 1 includes a brief introduction of ZnO nanostructures, motivation and problem statement, scope of study, thesis objectives, and originality of thesis.

Chapter 2 provides the literature review and theoretical background of the growth techniques, structural and electrical properties, and applications of ZnO and ZnO nanostructures.

Chapter 3 describes the general principles of equipment and techniques utilized for the synthesis and characterizations of aligned ZnO nanorods.

The synthesis processing of aligned ZnO nanorods and fabrication processing of UV photodetector device based on the ZnO nanorods are discussed in Chapter 4.

Chapter 5 presents the results related to the growth and characterizations of aligned ZnO nanorods grown on PEN substrate. Included are results on the effects of precursor concentration and growth time on morphology, structural, and optical characteristics of aligned ZnO nanorod arrays.

In Chapter 6, the effects of different growth parameters on the morphology, structural, and optical characteristics of aligned ZnO nanorod arrays synthesized on PS substrate are investigated and presented.

Chapter 7 focuses on the fabrication of UV photodetector using aligned ZnO nanorod arrays synthesized on flexible PEN and PS substrates and their optoelectronic properties.

Finally, the conclusions of this study and recommendations for future works are presented in Chapter 8.

CHAPTER 2

LITERATURE REVIEW AND BACKGROUND

2.1 Introduction

In this chapter, the description and type of nanomaterials, the structural and optical properties of ZnO materials will be addressed briefly. Next, the literature review and preparation parameters of ZnO nanorods by CBD method that influence on the crystalline quality and morphology of the ZnO nanorods will be discussed. The final part of this chapter will review the literature related to the UV photodetector based on ZnO nanorods. Furthermore, the basic theories of metal-semiconductor-metal photodetector and typical mechanism of photoconduction in ZnO nanorods are also described in this section.

2.2 Nanomaterials

Nanoscience and nanotechnology have developed at a huge speed and have gained substantial popularity for the last two decades. Materials that have at least one dimension at the nano-scale (1-100 nm) are called nanomaterials. Nanostructured materials contain quantum dots, nanoparticles (0-dimension), nanorods, nanotubes, nanowires (1-dimension), nanosheets, thin films (2-dimension), and nanospheres (3-dimension). Nanostructured materials have drawn great interest from researchers owing to their unusual mechanical, optical and electrical properties that are distinct from those of their bulk phases. Recent progress in nanostructured materials have opened up new various applications in energy, electronics, materials chemistry, catalysis, and even biology. Materials in the nanometer scale have unique physical and chemical characteristics, which are strongly dependent on the nanostructure size

and surface nature. These variations mainly arise from two effects. The first effect is the surface to volume effect, which occurs when the particle size decreases and the surface to volume ratio increased. Thus, the decrease of the particle size results in the increase of number of surface atoms in nanostructure material. The second effect is the quantum confinement effect, which happens once the particle size approaches the material exciton Bohr radius, where the optical and electronic properties of nanostructured material will considerably alter from the bulk nature [17]. Several types of synthetic methods have been used to produce the nanostructured materials. These techniques include the liquid phase techniques, gas phase methods, and mixed phase syntheses. The choice of suitable technique is important to determine the failure or success of the synthesized nanostructured materials, because physical and chemical properties and applications of nanomaterials are strongly dependent upon how they are fabricated. For several decades, the importance of selecting a suitable method in forming nanomaterials has been a motivating force for the development of new methodologies [18].

2.3 Overview of ZnO and ZnO nanostructures

ZnO is an intrinsically n-type semiconductor and transparent conducting oxide semiconductor material. ZnO nanostructures have received more attention of researchers because they have unique properties such as a great optical gain (which is more than that of GaN [19]), direct wide band gap of 3.37 eV (which is useful for photonic applications), and a high exciton binding energy of 60 meV (which is more than that of ZnSe (22 meV) and GaN (25 meV) [20]), which is useful for efficient excitonic emissions and lasing applications even at the temperature of room. ZnO is a versatile functional material that have been fabricated using diverse chemical and

physical fabrication methods in various group of growth morphologies, which include thin films, single crystals, powders, and nanostructures [21], such as nanoparticles, nanowires, nanorods, nanocombs, nanotubes, nanonails, nanosheets, nanobelts, and nanoflowers. These novel ZnO nanostructured materials have drawn great attention owing to their distinguished performance in optics electronics, and photonics. These novel nano-structural ZnO materials introduced novel electronic and optical properties, which are greatly believed to be the result of the quantum confinement effects and high surface to volume ratio [22]. The unique properties of the ZnO nanostructured materials have created wide range of applications such as chemical sensors, UV detectors, solar cells, piezoelectric and UV light emitting devices.

2.3.1 Crystal structures and lattice parameters of ZnO

Most of the group II–VI binary compound semiconductors crystallize into either hexagonal wurtzite or cubic zincblende structure where each cation is surrounded by four anions at the corners of a tetrahedron, and vice versa. ZnO is a semiconductor compound of the group-II element ${}_{30}\text{Zn}$ (with the electronic configuration $(1s)^2(2s)^2(2p)^6(3s)^2(3p)^6(3d)^{10}(4s)^2$) and the group-VI element ${}_{8}\text{O}$ (with the electronic configuration $(1s)^2(2s)^2(2p)^4$). Under ambient pressure and temperature, zinc oxide crystallizes in the hexagonal wurtzite-type structure and its phase is thermodynamically stable, as presented in Figure 2.1 (a) [23]. This hexagonal lattice of ZnO belongs to the space group of C_{6v}^4 in the Schoenflies notation, and is characterized by two interconnecting sublattices of O^{2-} and Zn^{2+} , such that each oxygen ion is surrounded by four zinc ions, and vice versa. The wurtzite structure consists a hexagonal unit cell with lattice parameters a and b lay in

the x - y plane (which include an angle of 120° and have equal length), and c is parallel to the z -axis, which are revealed in Figure 2.1 (b) [23]. Figure 2.2 exhibits several lattice planes and direction with their Miller indices in a hexagonal unit cell [24]. The lattice parameters values of the hexagonal unit cell at room temperature are $a = b \approx 3.2495 \text{ \AA}$ and $c = 5.2069 \text{ \AA}$. The axial ratio c/a of an ideal hexagonal wurtzite structure is $(8/3)^{1/2} = 1.633$, which changes in response to stress or strain [25]. Experimentally, for hexagonal wurtzite structure of ZnO, the real value of c/a was determined in the range $c/a = 1.593$ – 1.603 [26]. This tetrahedral coordination of wurtzite structure gives rise to polar symmetry along the hexagonal axis, chosen to be parallel to z . This polarity is responsible for a number of the properties of ZnO such as its spontaneous polarization and piezoelectricity, and is also an important factor in defect generation and crystal growth.

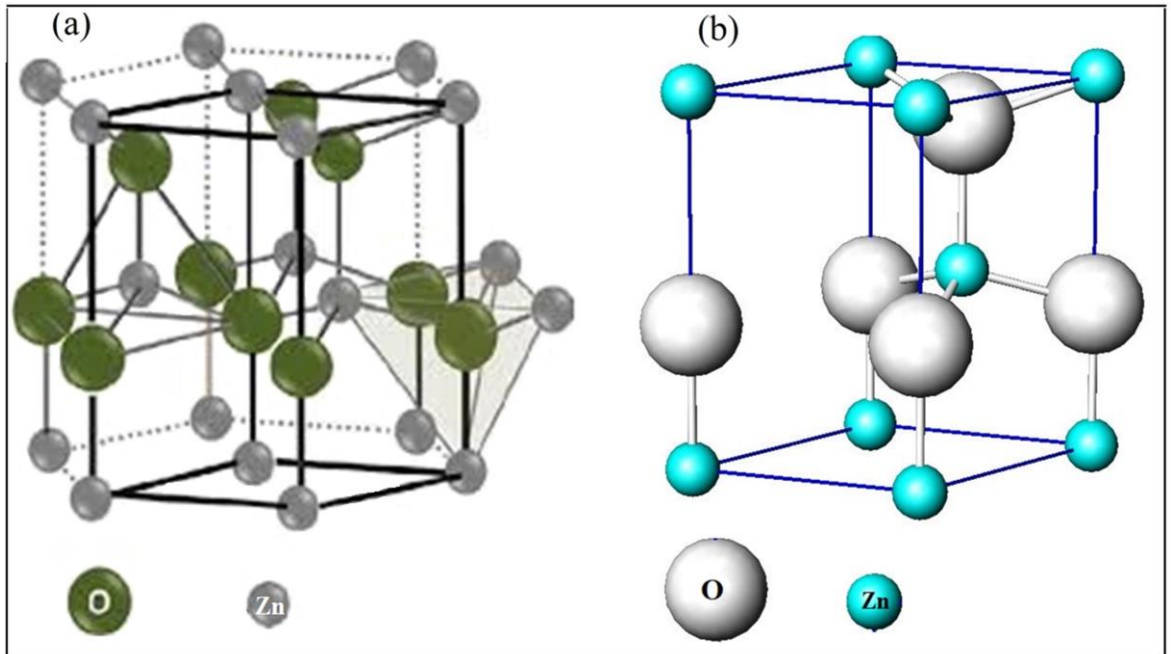


Figure 2.1: (a) The hexagonal wurtzite structure and (b) hexagonal unit cell of ZnO [23].

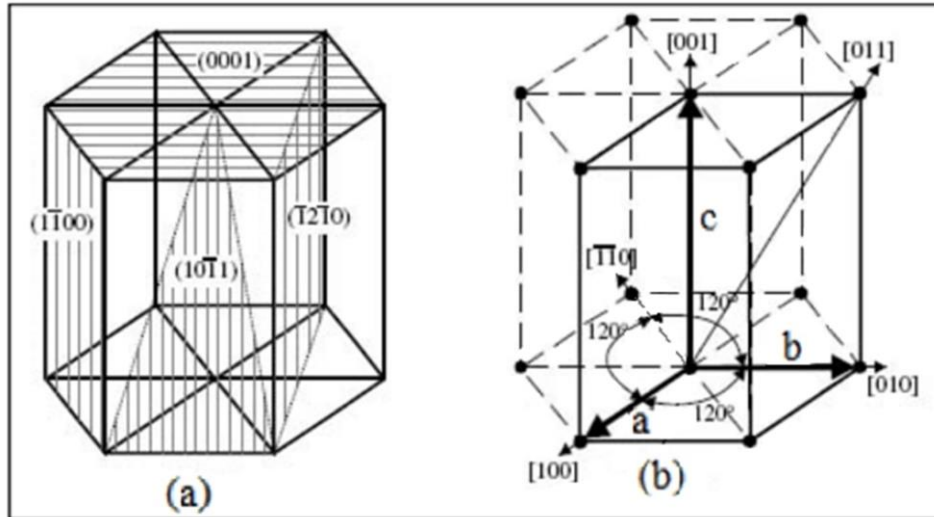


Figure 2.2: (a) Miller indices of several lattice planes in a hexagonal lattice of ZnO and (b) hexagonal unit cell and indices of several lattice directions [24].

In addition to the hexagonal wurtzite-type structure, ZnO also crystallizes in the rock salt (NaCl) and cubic zincblende structures, which are demonstrated in Figure 2.3 [23]. The rock salt type structure may be obtained at relatively high-pressure of ~ 10 GPa [27], whilst zincblende-type structures of ZnO is stable only by growth on substrate with cubic structure like ZnS [28].

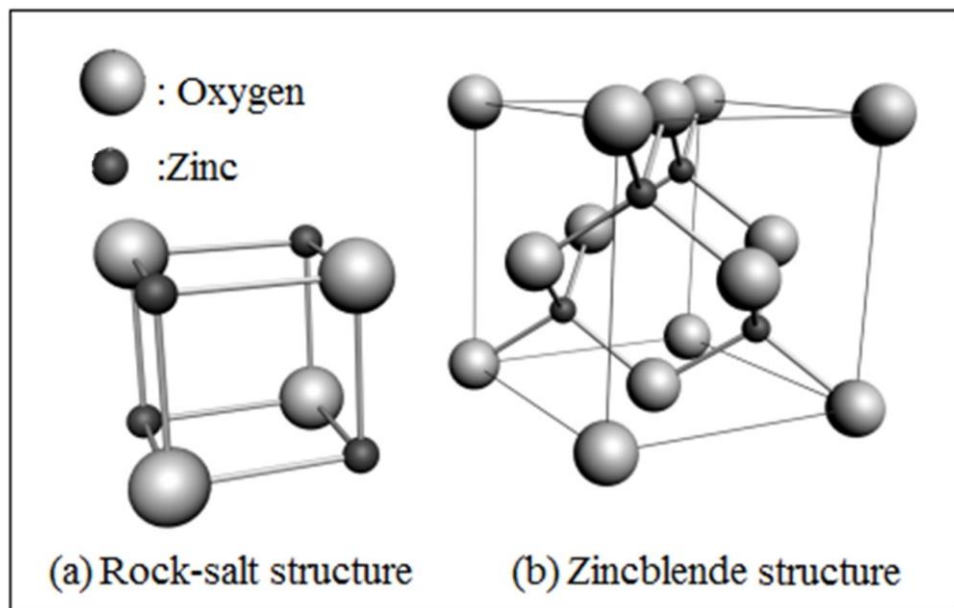


Figure 2.3: (a) The rock salt and (b) zincblende structures of ZnO [23].

2.3.2 Optical properties of ZnO

ZnO nanostructures are a promising semiconductor material. These nanostructures have a direct wide band gap of 3.37 eV useful for photonic applications, high exciton binding energy of 60 meV for efficient excitonic emission even at the temperature of room, large absorption coefficient at near band edge, and efficient radiative recombination. The majority of the optical transitions of ZnO nanostructures have been investigated using photoluminescence spectra at room temperature. PL spectra of ZnO nanostructure mainly consist of a UV emission (around 380 nm) owing to the near band edge of free exciton recombination and possibly a visible broadband emission (around 550 nm) because of impurities and/or defects. Displacements in the position of the PL peak of ZnO nanostructures with different sizes have been appeared in PL spectra. One possible reason for blue shift in the UV emission of ZnO nanostructures with decreasing size is the quantum confinement effects [29]. Different native defect concentrations have also been suggested as a reason for the variations in the position of the UV emission in different ZnO nanostructures with relatively large dimensions. The density of defects on the surface is larger than in the bulk [30], thus displacements in the position of the PL spectra due to the different concentrations of defects are expected to happen in nanostructures with various sizes because of different surface area-to-volume ratios. Therefore, the shape of the PL spectrum as well as the position of the UV emission could be affected by the defects density in nanostructures.

Even though there have been several reports of the PL spectra for ZnO nanostructures with strong UV emission and weak visible (defect) emission [1], in some instances the visible emission peak is higher than the UV emission peak [31] or only visible emission peak [32]. When the PL measurements of different ZnO

nanostructures were carried out under identical excitation conditions, the ratio of the UV peak intensity to the defect-related peak intensity can be characterized the crystalline quality of the ZnO nanostructures.

Several different peaks in the visible spectral region ranging from 405 nm to 640 nm have been appeared in PL spectra of ZnO nanostructure, which is attributed to the defect emission [33]. The deep-level emissions (DLE) in the visible range are owing to the recombination of photogenerated holes with singly ionized charge states in intrinsic defects, such as impurities, Zn interstitials, and oxygen vacancies [34]. Oxygen vacancies happen in three diverse charge states: singly ionized, doubly ionized, and neutral oxygen vacancies [35]. Zainizan et al. [36] reported indigo emission ranging from 405 nm to 440 nm which is attributed to electron transition from the conduction band to the oxygen interstitial, which is the acceptor defect in intrinsic ZnO. The blue emissions within 440 nm to 490 nm was generated from the electron transitions from the shallow donor level of zinc interstitials and oxygen vacancy to the valence band [37]. The green emission within 490 nm to 560 nm is the most usually observed defect emission in ZnO nanostructures, which is attributed to the defects of singly ionized oxygen vacancy. The yellow and orange emissions within 560 nm to 630 nm were generated from the electron transitions between the energy levels of the interstitial zinc and oxygen. The red emission within 630 nm to 700 nm is ascribed to the emissions combination attributed to the doubly ionized oxygen vacancy and interstitial oxygen [38].

2.4 Overview of substrates

To date, various substrate types have been used to synthesize ZnO nanostructures by different methods. The structural and surface morphology of

substrates and their lattice mismatch with nanostructures are significant parameters; because these factors control the nature and morphology of the fabricated ZnO nanostructures.

2.4.1 Flexible polyethylene naphthalate (PEN) substrate

Recently, many people are interested in devices, which are transparent, flexible, small volume and lightweight for portability and foldability. With these increasing demands for convenient and portable applications, flexible polymer substrates are more useful for flexible devices compared with conventional rigid substrates. Although flexible polymer substrates have limitation of deposition temperature for keeping its mechanical and chemical properties, applications of flexible polymer substrate have been attracted much attention because of their unique advantages such as transparency, transportability, lightweight, and high resistance to impact damage contrary to stainless steel and conventional rigid substrate. Therefore, the use of flexible polymer substrates is extensively studied for flexible optoelectronic, and elastic electronic devices devices such as smart cards [13], light emitting diodes [14], solar cells [15], and displays [16]. The flexible polymer substrates also have a low heat resistance at high temperature. Several types of polymer substrates such as polyethylene naphthalate (PEN), polycarbonate (PC), polyethersulfone (PES), polyimide (PI), and polyethylene terephthalate (PET) exist. Among these substrates, PEN is quite appropriated to be used in flexible optoelectronic and electronic devices because of its optical and mechanical properties such as its semicrystalline transparent polymeric property, melting temperature of 270 °C, higher processing temperature between 180 °C and 220 °C, high transparency (> 85%), high Young's modulus (6.1 GPa), and high tensile

strength (275 MPa) [39]. In addition, the use of flexible substrates to grow ZnO nanorods offers more benefits such as low cost and suitability for moving objects.

To date, many researchers have synthesized various ZnO nanostructures by different method on the PEN substrate. Kim et al. [40] synthesized multiple-stack high density ZnO nanorod/nanoflower structures by hydrothermal method on the as-prepared and plasma treated seed layer ZnO/PEN substrates. Bowen et al. [41] demonstrated the influence of thickness on the surface morphology, optical, structural, mechanical and electrical properties of F doped ZnO films on the PEN substrates deposited using radio frequency (RF) magnetron sputtering system at room temperature. Fonrodona et al. [42] reported Al doped ZnO layers deposited on PEN substrates using RF magnetron sputtering for low-temperature deposited solar cells. Tao et al. [43] synthesized Ga doped ZnO thin films on flexible PEN substrate using direct current (DC) magnetron sputtering system at room temperature. They investigated the effect of plasma and distance between substrate on the optoelectronic and structure properties of Ga doped ZnO, and the optimized Ga doped ZnO thin films used as front contacts for thin film silicon solar cells on PEN substrate at room temperature.

In the study, the quality and performance of ZnO nanorods UV photodetector on PEN are compared with ZnO nanorods UV photodetector grown on PS substrate.

2.4.2 Porous silicon (PS) substrate

Porous semiconductors have been extensively investigated in the past decades because of their adjustable roughness, low cost, and their special optical properties such as band-gap shift, improved photoresponse, and enhanced luminescence intensity [44]. Porous silicon (PS) nanostructures have been formed on Si wafer

using electrochemical etching of Si in hydrofluoric acid solution. PS is intensively studied among porous semiconductors because PS has a large internal surface area, high resistivity, strong surface absorbability, and applications in developing silicon-based optoelectronic devices [45]. PS layers can reduce large mismatches in lattice constants, and thermal expansion coefficients, thus reducing the large stress between ZnO nanostructures and Si substrates [46, 47]. The combination of ZnO nanostructures and porous silicon substrate can be considered as a white light source generated from the red emission from the PS layers and with green and blue-UV emissions from the ZnO nanostructures [48]. ZnO/PS layers also exhibit superior luminescence properties that satisfy the optical and electrical requirements of display technologies. Moreover, various kinds of ZnO nanostructures have been synthesized by different methods on PS substrates. For example, Rajabi et al. [49] reported the influence of surface roughness of substrate on structural morphology of ZnO rods grown on oxidized PS and PS substrates by vapour-phase transport method. Hsu et al. [47] reported the enhancement of ZnO nanowire orientation on PS substrate using a vapor–liquid–solid method. Abdulgafour et al. [50] fabricated a nanocoral reef of ZnO on PS substrates with no catalyst via the simple thermal evaporation method. Rusli et al. [51] prepared the high density ZnO nanorods using a thermal evaporation technique with no catalyst on PS substrates at growth temperatures ranging from 600 °C to 1000 °C. Rajabi et al. [52] synthesized ZnO tetrapods and nanorods on PS substrate without and with an Au catalyst using the chemical vapour transport and condensation method.

2.5 Overview of chemical bath deposition technique

2.5.1 The chemical bath deposition technique

Several techniques have been used for the synthesis of ZnO nanostructures on various kinds of substrates that can be categorized as a vapor-based technique and a solution-based technique. Vapor-based technique includes vapor–liquid–solid, thermal evaporation, metal organic chemical vapor deposition, chemical vapor deposition, molecular beam epitaxy, and chemical vapor transport and condensation method. Although vapor-based techniques can produce high quality ZnO nanostructures under well controlled high-vacuum conditions, these techniques however have several disadvantages such as high temperature, high cost of equipments, complexity, and are not suitable for growth of ZnO nanostructures on flexible plastic substrates due to the high growth temperature [53].

Solution-based technique includes solvothermal method, hydrothermal method, chemical bath deposition, and electrochemical deposition. The solution-based technique has been utilized greatly for mass production of oxide nanomaterials, semiconductors, and metals with good controls of the morphology and composition because of its low-temperature process, more environmentally friendly chemicals used, simplicity, lower cost, and capability for large-scale production. Solvothermal reactions include the use of organic or inorganic (non-aqueous) as a solvent to prepare materials under high pressure and temperature. The process is called hydrothermal when water as a solvent is used instead of organic or inorganic solvents to form materials at pressures ranging from 10^6 Pa to 10^8 Pa and temperatures ranging from 100 °C to 1000 °C in a closed vessel [54]. When water is utilized as a solvent of the starting materials under ambient pressure and temperature lower than 100 °C, the method is called chemical bath deposition. Electrochemical deposition is similar to CBD except that the substrate is placed onto an electrode and electricity is applied for the deposition of materials on the substrate.

Unlike vapor-based techniques and electrochemical deposition, CBD can be utilized at low temperature for broad variety of substrates such as non-conductive surface, plastic, and polymer (because these substrates have low heat resistance at high-temperature processes).

To date, CBD is widely used to fabricate various kinds of nanostructured semiconductor materials with high crystallinity, good optical and electrical properties in varied morphologies such as nanoparticles, nanocrystalline thin films, nanobelts, nanotubes, nanoflowers, nanowires, and nanorods. The morphology, structural, and optical properties of these nanostructured semiconductor materials can be controlled via numerous growth parameters, such as precursor type, precursor concentration, duration and temperature of growth.

In 1835, for the first time deposited silver thin film using CBD for mirror application [55]. Bruckman et al. used starting salt materials such as sodium hydroxide, thiourea ($\text{SC}(\text{NH}_2)_2$), and lead acetate by CBD to prepare thin films of lead sulfide (PbS) in 1933 [56]. Vayssieres et al. reported synthesis of ZnO microrod arrays by CBD on transparent conducting tin oxide glass substrate using zinc nitrate tetrahydrate ($\text{Zn}(\text{NO}_3)_2 \cdot 4\text{H}_2\text{O}$) and methenamine ($\text{C}_6\text{H}_{12}\text{N}_4$) for the first time in 2001 [57]. In 2004, Peterson et al. synthesized ZnO nanocolumns by CBD on sputter-coated ZnO substrates using sodium hydroxide (NaOH) and zinc nitrate hexahydrate ($\text{Zn}(\text{NO}_3)_2 \cdot 6\text{H}_2\text{O}$) [58]. To date, several researchers have been investigated diverse morphologies of ZnO nanostructures grown using CBD method on different substrates. Table 2.1 summarizes the various types of ZnO nanostructures synthesized by CBD on different kinds of substrates.

Table 2.1: Summary of the ZnO nanostructures synthesized using CBD method.

ZnO nanostructures	Type of starting materials	Substrate	Ref.
Individual ZnO nanorods	Zinc nitrate hexahydrate and ammonium hydroxide	Silicon	[60]
Self-assembled ZnO nanorods	Zinc nitrate hexahydrate and hexamine	Pre-treated silicon	[61]
ZnO nanorods	Zinc nitrate hexahydrate and hexamethylenetetramine	Silicon	[62]
ZnO nanorods	Zinc nitrate hexahydrate and hexamethylenetetramine	p-type porous silicon	[63]
ZnO nanoneedle and nanorods	Zinc nitrate hexahydrate and hexamethylenetetramine	Fluorine doped tin oxide (FTO)	[64]
ZnO nanorods	Zinc acetate dehydrate and hexamethylenetetramine	Silicon	[65]
ZnO nanorods	Zinc acetate and hexamethylenetetramine	Graphite	[66]
ZnO nanorods	Zinc chlorate and hexamethylenetetramine	Glass	[67]

2.5.2 Mechanism of chemical bath deposition technique

The mechanism of CBD method for growth of ZnO nanorods in a process of hydrolysis and precursors condensation can be described as follows. In this method, a substrate is dipped vertically inside a beaker containing the aqueous solution of hexamethylenetetramine ($C_6H_{12}N_4$) and zinc nitrate hexahydrate that act as a source of OH^- and Zn^{2+} ions, respectively. Colloidal $Zn(OH)_2$ clusters, which are necessary for the growth units of ZnO nanorod arrays, are produced from Zn^{2+} and

OH^- ions. The reactions involved in ZnO nanorod growth can be described by the following equations [59]:



2.6 Overview of ZnO nanorods growth conditions

2.6.1 Mechanism of ZnO nanorods growth conditions

Aligned ZnO nanorod arrays will play an important role in a wide range of applications in the future optoelectronic devices. The structural, electrical and optical properties of the ZnO nanorod arrays strongly depend on the morphology and shape of the one-dimensional ZnO nanorods. Consequently, thorough understanding of the effects of growth parameters on morphology, size, and growth mechanism of ZnO nanorod arrays are essential. The mechanism for the influence of growth time and precursor concentration of ZnO nanorods can be explained based on the reactions of chemical in the CBD process and theory of nucleation and growth of ZnO crystal. In the chemical process of ZnO nanorods growth, $Zn(NO_3)_2 \cdot 6H_2O$, water molecules and $C_6H_{12}N_4$ in the solution provide Zn^{2+} , O^{2-} and OH^- ions, respectively [68]. The chemical reactions related to the growth process of ZnO nanorod arrays in CBD method (mentioned in previous section, i.e. Eq. 2.1 to Eq. 2.5) can be controlled through changing the parameters of reaction including growth time, growth

temperature, and precursor concentration. Wurtzite structure of ZnO nanorods has two types of crystal planes including polar (0 0 1) plane, and nonpolar planes such as (1 0 1) and (1 0 0). The crystal planes with greater surface energy have faster growth rate, as a result, the growth rate of the planes in the [0 0 1] direction is more than that of the planes in the [1 0 0] direction [69]. The aspect ratio of the as grown ZnO nanorods will be determined by the relative growth rate of the polar surface and non-polar surface [70].

However when the precursor concentration is increase the amount of $Zn(OH)_2$ that is generated from the precursor solution will also increase, and this leads to an increase in the growth rate of ZnO during CBD synthesis [70]. The endothermic nature of this process prevents the growth of ZnO nanorod arrays in the [0 0 1] directions, and thus ZnO nanorod arrays with thicker diameter and shorter length are fabricated with greater precursor concentration. The growth time dependence of the chemical reaction is another important parameter, which reflects the kinetics and/or thermodynamics processes due to its close relation to the reaction rate and concentration change in the reaction process [71]. With the increase of growth time, the polar (0 0 1) plane will be dissolved from the top of ZnO nanorods to form hexagonal volcano-like ZnO nanorods [69].

2.6.2 Literature review

Li et al. [70] synthesized ZnO nanorod arrays on Si substrate by CBD technique and investigated systematically the effect of temperature, duration of growth and precursor concentration on morphology of the ZnO nanorod arrays. They found that the average length of ZnO nanorod arrays increased with increasing precursor concentration from 0.125 M to 0.250 M and then decreased with further

increased precursor concentration up to 0.500 M, while the average diameter and aspect ratios of ZnO nanorod arrays increased and decreased with increased precursor concentration from 0.125 M to 0.500 M, respectively. Moreover, they found that the average length and diameter of ZnO nanorod arrays increased when the growth duration continues to increase from 3 h to 5 h. No considerable change on morphology and average diameter of ZnO nanorod arrays was observed for growth duration of 7 h or 9h.

Yang et al. [65] used the two-step chemical bath deposition method to fabricate vertically ZnO nanorod arrays on Si substrate with different diameters. The results showed that the density and orientation of ZnO nanorods were almost the same for all growth time and the average diameter of the aligned ZnO nanorod arrays increased with increased duration of growth from 2h to 5h. Amin et al. [72] studied the influence of growth time and precursor concentration on the morphology of hydrothermally synthesized ZnO nanostructures on Si substrate. They concluded that the prepared ZnO nanostructures with precursor concentration from 0.005 M to 0.025 M, from 0.050 M to 0.300 M, and more than 0.400 M change nanowires to nanorods and finally convert to a polycrystalline thin film. In addition, the diameter of ZnO nanorod arrays increased gradually with increasing of the precursor concentration, while the length of ZnO nanorods becomes constant for precursor concentration more than 0.200 M. Moreover, they found that the ZnO nanorods had a steady and continuous growth (increase in the diameter and length) up to growth time of 10 h and then the length and diameter of ZnO nanorod arrays decreased gradually with increasing growth time to 20 h.

Terasako et al. [67] systematically studied the effect of precursor concentration on the morphology and photoluminescence properties of aligned ZnO

nanorod arrays synthesized on seed layer Au/glass substrate by CBD method from the aqueous solution of zinc chloride and the mixed aqueous solution of hexamethylenetetramine and zinc acetate dehydrate. Jeonga et al. [71] studied the effect of growth time on the morphology, structural and optical properties of vertically aligned ZnO nanorod arrays synthesized by solution growth method on Si and flexible PET substrates. They found that with increasing of the growth time from 1 h to 5h, the average diameter of synthesized ZnO nanorod arrays on ZnO/PET substrate increased, and then the increase of diameter of ZnO nanorod arrays stopped when the growth time continues to increase to 10 h. In addition, they found from the PL and XRD results that the optical and structural properties of aligned ZnO nanorod arrays grown after growth time of 6 h and 5 h were most improved, respectively. Ko et al. [73] synthesized vertically aligned ZnO nanorod arrays on seed layer ZnO/indium tin oxide (ITO) coated PET substrate by electrochemical deposition technique and investigated the morphology and optical properties of ZnO nanorod arrays using changing the zinc nitrate concentration. Shin et al. [74] investigated the effect of growth duration on the morphology, optical and structural properties of ZnO nanorod arrays synthesized by hydrothermal method on seed layer ZnO/PES substrates.

2.7 Overview of ultraviolet (UV) photodetection based on ZnO nanorods

UV photodetectors that have been fabricated in different kinds such as metal-semiconductor-metal structures, p-n junctions, and Schottky diodes [75-77] are essentially semiconductor devices that generate photocurrent through the conversion of optical energy (UV light) into electrical energy. MSM UV photodetectors have been widely used in the field of optical communication applications in the past few

years because of the high response speed, which depends on the structure geometry. ZnO materials are suitable for UV photodetectors because of the direct wide band gap (3.37 eV), chemical stability, large exciton binding energy (60 meV), and biocompatibility.

In addition, ZnO nanostructured materials have unique characteristics as compared with bulk materials because of their novel chemical, mechanical, optical, and electrical properties, which resulted from the quantum confinement effects and high surface area to volume ratio or a combination both [17], and have been broadly studied in optoelectronic applications. ZnO nanorods can be assumed to be excellent nanostructure materials for detection of UV light compared to bulk materials due to their high-quality single-crystal nanorods and high surface area to volume ratio of nanorods.

2.7.1 Literature review

Photodetector was studied for the first time in 1873, when photoconductivity was discovered in selenium by Smith [78]. ZnO nanostructured materials are sensitive to UV illumination because of the direct wide band gap and large exciton binding energy at room temperature [79]. ZnO nanostructures can be easily synthesized in various morphology such as nanorods or nanowire, and the strong photoresponse make them promising materials for optoelectronic and optical applications.

First studies on UV photodetector based on ZnO nanowire can be dated back to 2002 when Kind et al. [80] found that the conductivity of a single ZnO nanowire strongly depends to the UV illumination. The performance of UV photodetectors based on their applications refers to sensitivity, response and recovery times,

wavelength selectivity, and quantum efficiency [81]. To date, many researchers have fabricated the 1D ZnO UV photodetectors based on different device structures including individual nanowire/nanorod, lateral nanowires/nanorods, multiple horizontal nanowires/nanorods, vertical aligned nanowires/nanorods, and etc.. The device structure, substrate, illuminated UV wavelength, applied bias voltage, response time, and recovery time of some of 1D UV photodetectors are summarized in Table 2.2.

2.7.2 Theoretical concepts of ultraviolet (UV) detection

Photodetectors have attracted great attention because of their important roles in the development of optical communication systems. The main physical mechanism of photodetectors is based on the absorption of photons with energy more than the energy gap of the semiconductor, which alters the electric properties of the electronic system, such as the creation of a photovoltage in a photovoltaic detector or a photocurrent in a photoconductor.